Deletion of the Helical Motif in the Intestinal Fatty Acid-Binding Protein Reduces Its Interactions with Membrane Monolayers: Brewster Angle Microscopy, IR Reflection-Absorption Spectroscopy, and Surface Pressure Studies†

Fangjun Wu,‡ Betina Corsico,§ Carol R. Flach,‡ David P. Cistola,|| Judith Storch,*,§ and Richard Mendelsohn*,‡

Department of Chemistry, Newark College of Arts and Science, Rutgers University 73 Warren Street, Newark New Jersey, 07102, Department of Nutritional Sciences, Thompson Hall, Cook College, Rutgers University, New Brunswick, New Jersey 08901, and Department of Biochemistry & Molecular Biophysics, Washington University School of Medicine, 660 South Euclid Avenue, St. Louis, Missouri 63110

Received September 25, 2000; Revised Manuscript Received December 5, 2000

ABSTRACT: Intestinal fatty acid binding protein (IFABP) appears to interact directly with membranes during fatty acid transfer [Hsu, K. T., and Storch, J. (1996) *J. Biol. Chem. 271*, 13317−13323]. The largely α-helical "portal" domain of IFABP was critical for these protein−membrane interactions. In the present studies, the binding of IFABP and a helixless variant of IFABP (IFABP-HL) to acidic monolayers of 1,2-dimyristoylphosphatidic acid (DMPA) has been monitored by surface pressure measurements, Brewster angle microscopy (BAM), and infrared reflection−absorption spectroscopy (IRRAS). Protein adsorption to DMPA exhibited a two phase kinetic process consisting of an initial slow phase, arising from protein binding to the monolayer and/or direct interfacial adsorption, and a more rapid phase that parallels formation of lipid-containing domains. IFABP exhibited more rapid changes in both phases than IFABP-HL. The second phase was absent when IFABP interacted with zwitterionic monolayers of 1,2-dipalmitoylphosphatidylcholine, revealing the important role of electrostatics at this stage. BAM images of DMPA monolayers with either protein revealed the formation of domains leading eventually to rigid films. Domains of DMPA/IFABP-HL formed more slowly and were less rigid than with the wild-type protein. Overall, the IRRAS studies revealed a protein-induced conformational ordering of the lipid acyl chains with a substantially stronger ordering effect induced by IFABP. The physical measurements thus suggested differing degrees of direct interaction between the proteins and DMPA monolayers with the IFABP/DMPA interaction being somewhat stronger. These data provide a molecular structure rationale for previous kinetic measurements indicating that the helical domain is essential for a collision-based mechanism of fatty acid transfer to phospholipid membranes [Corsico, B., Cistola, D. P., Frieden, C. and Storch, J. (1998) *Proc. Natl. Acad. Sci. U.S.A. 95*, 12174−12178].

The mammalian fatty acid binding proteins (FABPs) consist of a family whose putative functions include intracellular uptake and transport of amphipathic lipids such as long-chain fatty acids and retinoids (*1*, *2*). IFABP is abundant in polarized intestinal columnar epithelial cells (enterocytes), and is proposed to be important for intracellular trafficking and processing of the large quantities of dietary fatty acid absorbed by the small intestine (*3*). It has a molecular weight of 15100 and is composed of a 10-stranded, antiparallel β-barrel formed by two β-sheets stabilized by intrastrand H-bonds. The IFABP ligand-binding cavity is enclosed by the two β-sheets and is capable of accommodating the long chain fatty acid, fundamental to the presumed physiological role of the protein. Interestingly, the interior space (1000 Å^3) is substantially larger than that required for the binding of a single molecule of fatty acid (300 Å^3); however, biochemical and structural studies demonstrate a 1:1 stoichiometry (*4*, *5*). Water molecules in the cavity stabilize the structure by forming H-bonds with the internal polar side chains (*6*). A short helix-turn-helix motif exists between β-strands A and B. The first α helix is amphipathic. The helical domain plus closely positioned β-turns are referred to as the "portal" through which fatty acids are believed to enter and exit the binding cavity (*7*, *8*).

Hsu and Storch (*4*) discovered that fatty acid transfer from IFABP to acidic membranes occurred via a collisional

† This work was supported by PHS Grants GM 29864 (R.M.), DK38389 (J.S.), DK52574 (D.P.S.), and DK 48046 (D.P.S.).

* To whom correspondence should be addressed. (R.M.) Phone: (973) 353-5613. Fax: (973) 353-1264. E-mail: mendelso@andromeda.rutgers.edu. (J.S.) Phone: (732) 932-1689. Fax: (732) 932-3769. E-mail: storch@aesop.rutgers.edu.

‡ Department of Chemistry, Newark College of Arts and Science, Rutgers University.

§ Department of Nutritional Sciences, Thompson Hall, Cook College, Rutgers University.

|| Department of Biochemistry & Molecular Biophysics,Washington University School of Medicine.

[1] Abbreviations: A/W, air/water; BAM, Brewster angle microscopy; DMPA, 1,2-dimyristoylphosphatidic acid; DMPC, 1,2-dimyristoylphosphatidylcholine; DOPC, 1,2-dioleoylphosphatidylcholine; DPPC, 1,2-dipalmitoylphosphatidylcholine; IFABP, intestinal fatty acid binding protein; IFABP-HL, helixless variant of IFABP; IRRAS, infrared reflection−absorption spectroscopy; FABP, fatty acid binding protein; $\nu_s(CH_2)$, CH_2 symmetric methylene stretching frequency; LC, liquid-condensed; LE, liquid-expanded; NMR, nuclear magnetic resonance.

10.1021/bi002252i CCC: $20.00
Published on Web 01/26/2001

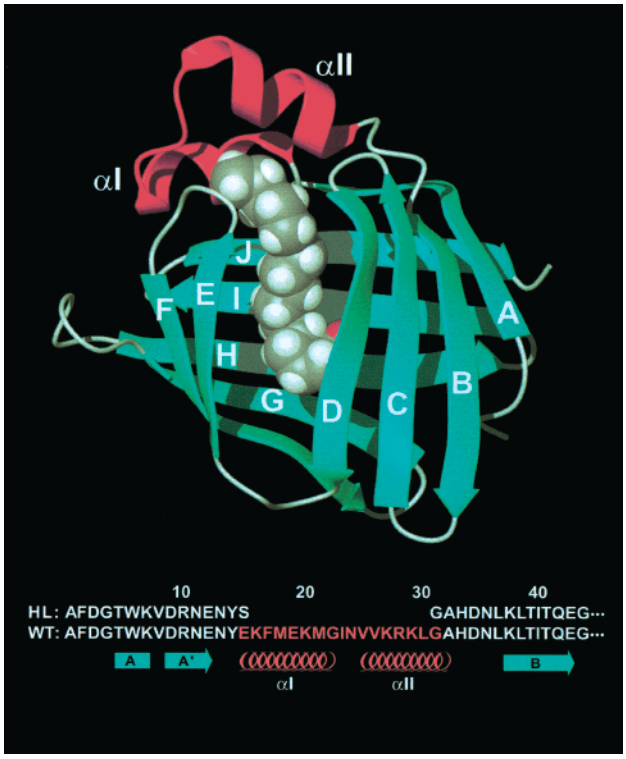

FIGURE 1: Structure of wild-type holo rat IFABP as determined by NMR spectroscopy (*9*). An N-terminal sequence alignment of the wild-type (WT) and helixless (HL) variant is included. The helix-less variant was engineered by deleting residues 15−31 spanning the helix-turn-helix domain (pink) and replacing it with a two-residue Ser-Gly linker.

mechanism involving transient ionic and hydrophobic interactions, with the rate of ligand transfer dramatically enhanced to acidic membranes in particular. This finding explained the much enhanced transfer rate for IFABP compared with liver FABP, in which the transfer was diffusion-based. An analogous collision-based mechanism was found for adipocyte and heart FABP. Neutralization of the surface lysine residues reduced the transfer of fatty acids from adipocyte FABP to membranes (*5*). Furthermore, point mutations in heart FABP demonstrated that portal domain lysine residues were critical for effective collisional interactions (*6*).

Figure 1 illustrates the structure of wild-type holo rat IFABP as determined by NMR spectroscopy (*9*). A helix-less variant of IFABP (IFABP-HL) was engineered by deleting residues 15−31 spanning the helix-turn-helix domain (magenta) and replacing it with a two-residue Ser-Gly linker (*10*). The NMR structure of IFABP-HL retains the β-sheet topology of the wild-type protein, but lacks the helices (*11*). The deletion of the helical domain resulted in a large opening that connects the interior ligand-binding cavity with exterior solvent. One fatty acid molecule binds to IFABP-HL with an orientation similar to that for the wild-type protein (*12*). Unlike the wild-type protein, fatty acid dissociation from IFABP-HL is structurally and kinetically unimpeded (*11*, *12*).

Recently, the membrane transfer properties of IFABP-HL were compared with those of the wild-type protein (*13*). These kinetic studies suggested that fatty acid transfer from helix-less IFABP to acceptor bilayers did not involve a collisional mechanism, further supporting the importance of the helical domain for protein−membrane interactions. The availability of IFABP-HL makes it feasible to compare it to the wild-type protein with respect to direct membrane interactions.

Lipid monolayers provide a useful experimental paradigm for the investigation of lipid/protein interaction. In addition to the traditional pressure−area (Π-A) or pressure−time isotherms, direct images of monolayer phases have been achieved by various types of optical microscopy. In particular, fluorescence microscopy (*14*) is widely used in this context to envision domain shapes and textures. The method provides excellent spatial resolution and contrast albeit occasionally suffering from artifacts when the concentration of fluorophore is high in a particular phase or from problems arising from heating of the fluorophore.

BAM provides information similar to fluorescence microscopy without the artifacts mentioned above (*15*). The approach is based on the characteristics of the reflectivity of light at the Brewster angle (α_B) as defined by

$$\tan \alpha_B = n_2/n_1$$

where n_1 and n_2 are refractive indices of two media at the Fresnel interface. In the case of the A/W interface, medium 1 is air and medium 2 the aqueous subphase. At the Brewster angle, the reflectivity of p-polarized (electric field parallel to the plane of incidence) light reaches a minimum. This phenomenon depends on the interfacial properties. If the refractive index in certain regions of the subphase is altered (e.g., by the presence of a lipid film) the difference in reflectivity thereby generated forms the basis for image contrast. IRRAS complements BAM in that it provides direct information about the conformational states of the hydrocarbon chains and the secondary structures of proteins adopted at the air/water interface.

The current study addresses the role proposed for the IFABP helix-turn-helix motif in membrane interaction by comparing the membrane binding behavior of wild-type IFABP and IFABP-HL to monolayers of DMPA, using BAM, IRRAS and surface pressure techniques. DMPA was employed as a model acidic phospholipid whose phase behavior in monolayers is well documented and whose domains are effectively visualized (*16*). To simplify interpretation of data from monolayers, apo-IFABP and apo-IFABP-HL (no bound fatty acids) were used throughout.

EXPERIMENTAL PROCEDURES

Materials. DMPA, DOPC, and DPPC were obtained from Avanti Polar Lipids (Birmingham, AL). Recombinant IFABP and IFABP-HL were purified as previously described (*4*, *13*). HPLC-grade H_2O, chloroform, and methanol were purchased from Fisher Scientific (Pittsburgh, PA). D_2O (99.9% isotopic enrichment) was supplied by Isotec (Miamisburg, OH). All other chemicals were obtained from Sigma (St. Louis, MO) and were of the highest purity commercially available.

BAM Images of Monolayers. A Nima Technology (Coventry, U.K.) 601M Langmuir−Blodgett trough (98.6 cm^2 maximum area) equipped with a Model PS-4 tensiometer was used. The temperature of the subphase was controlled at 21.0 ± 0.5 °C. A total of 7.6 μL of the DMPA stock solution (1.18 mg/mL in chloroform) was spread with a Hamilton 10 μL microsyringe yielding an area of 1.09 nm^2/molecule. After an initial relaxation period of 30 min, the film was compressed continuously at a speed of 2.27 × 10^{-2}

nm^2/(molecule min). Unless otherwise indicated, this speed was utilized for all measurements. The subphase composition was 100 mM NaCl and 2 μM EDTA (pH 5.6). In the case of D_2O subphases, the pD was adjusted to 5.6.

A NFT MiniBAM (Göttingen, Germany) was aligned perpendicular to the compression direction. The polarizer and analyzer were set to p-polarization and the incoming laser light (688 nm, 30 mW) was fixed to an angle of incidence of 52−54° (Brewster angle for aqueous subphases). Images captured by a low geometrical distortion, sensitive, black/white frame transfer CCD camera were transferred in real time to a computer using a Univision (Burlington, MA) Scorpion 8G frame grabber card. The images were digitized (8-bit TIFF file) and analyzed with Image-Pro Plus 3.0 software (Media Cybernetics, Silver Spring, MD). BAM images were acquired at 1 min intervals in time-dependent measurements and were cut to the desired size; no other manipulations were made.

Protein Injection Techniques for BAM and Π*-Time Isotherms.* For protein adsorption experiments at the A/W interface, a DMPA monolayer was compressed to the onset of the LE/LC transition. The monolayer was allowed to equilibrate for at least 10 min prior to protein injection. To minimize changes of subphase volume and height, the volume of protein solution injected was controlled at 100 μL. The final concentration for IFABP in the subphase was ~0.2 μM. Since no stirring device was incorporated in our troughs, the postinjection kinetics were controlled solely by diffusion.

Bulk Phase IR Techniques. Protein concentrations ranged from 6 to 10 mg/mL in D_2O-based buffer solutions. Spectra were collected on a Mattson Instruments Research Series (RS-1) spectrometer equipped with an MCT detector and a sample shuttle. The spectrometer was under constant dry air purge. Samples were placed between CaF_2 windows separated with a 25 μm spacer. The typical amount of sample loaded was 25−30 μL. A thermostated transmission cell (Harrick Scientific, Ossining, NY) was used. Temperature was varied between 25 and 70 °C in increments of 5 °C. Spectra were obtained at ~4 cm^{-1} resolution by co-addition of 1024 interferograms. These were apodized with a triangular function, and Fourier transformed with two levels of zero filling, yielding spectra encoded every ~1 cm^{-1}. Eight blocks of 128 scans of sample and air background were co-added into separate files and ratioed producing IR spectra with optimal water vapor compensation.

IRRAS Measurements at the A/W Interface. The experimental setup has been described in detail previously (*17*). Briefly, the angle of incidence was set to 35° and unpolarized radiation was used. An optical filter (OFC Corporation, Natick, MA) was positioned in the incident light path to reduce heating effects of the IR beam (*18*). 1024 scans acquired with a resolution of 4 cm^{-1} were co-added and Fourier transformed with one level of zero filling to yield spectra encoded every 2 cm^{-1}. The temperature of the subphase was controlled at 21 ± 0.5 °C. A home-built trough with a maximum area of 86 cm^2 was utilized. The monolayer was discontinuously compressed over a time period of 3 h. The acquisition time for one spectrum was ~8 min. It took 4−5 h to complete a typical injection experiment. To optimize the water vapor compensation, 8 blocks, 128 scans each, of the film-covered and the film-free sides were taken alternatively, co-added, and their ratios calculated. In some cases, water vapor spectra were generated by calculating the ratio of two consecutive single beam IRRAS spectra of the film-free subphase. These were used to subtract the contribution of uncompensated water vapor from the film-covered subphase.

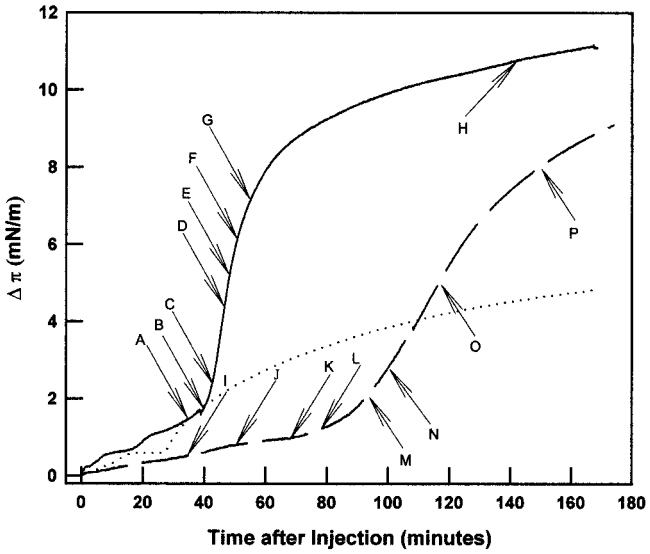

FIGURE 2: Surface pressure changes after injection of IFABP or IFABP-HL underneath a DMPA or DPPC monolayer at the onset of LE/LC coexisting region. IFABP injection beneath DMPA shows a ~40 min lag time followed by a cooperative increase in π. IFABP-HL injection beneath DMPA shows a longer lag time and more gradual increase in π. Legend: (—) IFABP (beneath DMPA monolayers); (− − −) IFABP-HL (beneath DMPA monolayers); (•••) IFABP (beneath DPPC monolayers). The letters refer to time points at which BAM images (Figure 3) were collected.

IR Data Reduction Protocols. The precise values of ν_s-(CH_2), and components of the protein amide I contour were determined with a center of gravity algorithm written by D. Moffatt and provided by the National Research Council of Canada. Spectral subtraction and baseline leveling were carried out with Grams/32 software (Galactic Industries Corporation, Ithaca, NY).

RESULTS

Surface Pressure and BAM studies of IFABP and IFABP-HL Interaction with DMPA. Changes of surface pressure with time following injection of wild-type IFABP and IFABP-HL beneath a DMPA monolayer are depicted in Figure 2. Following the injection, Π-time curves for both the wild-type and the helixless variants each reveal two kinetic phases. The first phase shows small linear increases in π. For IFABP this phase dominates for ~40 min, compared with the ~85 min period for IFABP-HL. The rate of surface pressure increase in the second kinetic phase is ~ 0.33 mN/m min for IFABP, and is significantly more rapid than the rate observed for IFABP-HL (~ 0.12 mN/m min). To elucidate the effects of lipid headgroup charge on the interaction with IFABP, wild-type protein was injected underneath a zwitterionic DPPC film at the onset of the LC/LE two phase coexistence region. Although it might have been appropriate to use DMPC (same chain length as DMPA) as a control for this purpose, monolayers of this material form only expanded phases at the temperature of the current experiment

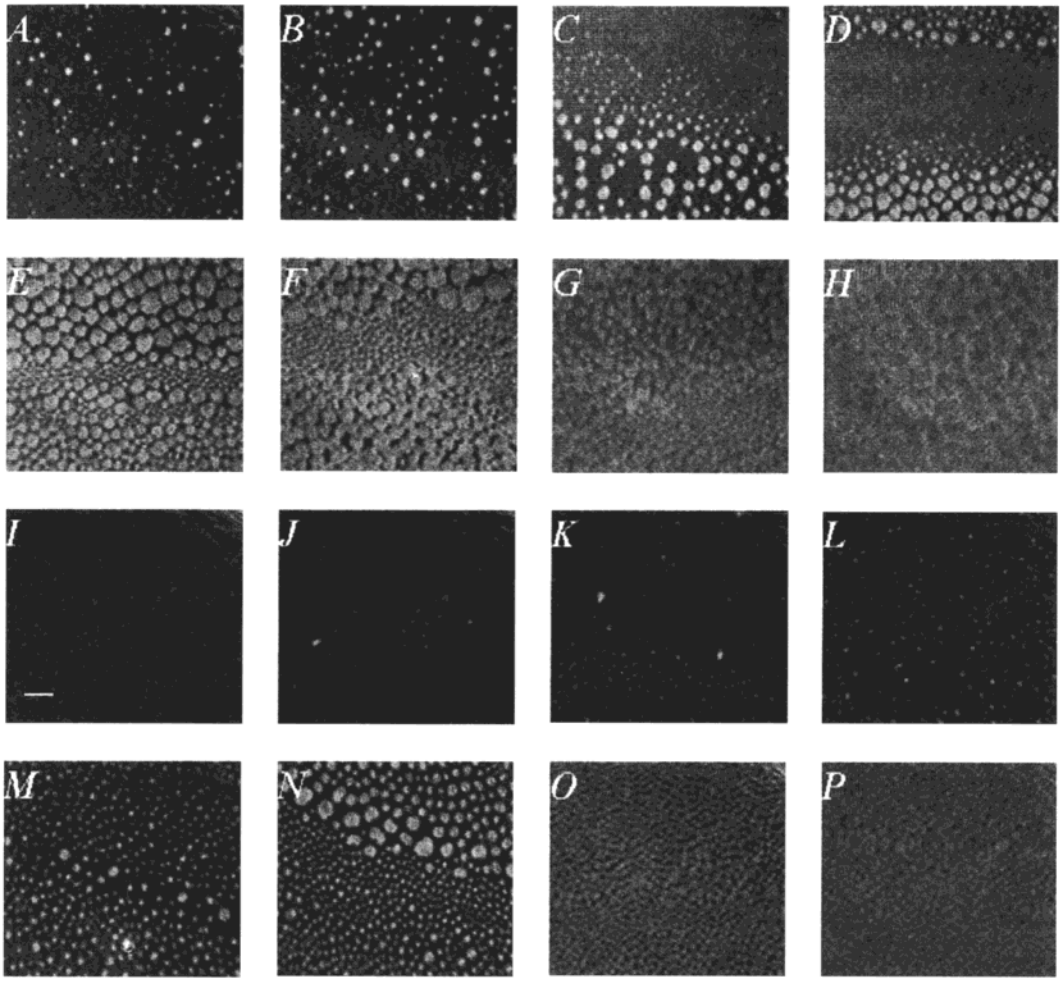

FIGURE 3: BAM images acquired at the $\Delta\pi$/time values marked in Figure 2. Images A−H are captured after IFABP injection, while images I−P are captured after IFABP-HL injection. The scale bar in image I is 250 μm and is appropriate for all images.

and thus have quite different physical characteristics from DMPA. The overall pressure change for protein injections under DPPC is much reduced relative to injections beneath DMPA monolayers, $\Delta\pi$ reaching only 4.5 mN compared with ~11 mN in the DMPA case. The second kinetic phase is absent in the IFABP/DPPC film, indicating that this stage of the IFABP/phospholipid interaction is controlled by electrostatic forces.

BAM images acquired as a function of time after injection of each protein beneath monolayers of DMPA are displayed in Figure 3. In the wild-type case, small domains are detected close to the onset of the second kinetic phase, (Figure 3A). With increasing π, at ~38 min, domains grow both in size (Figure 3C) and density (Figure 3E). The distribution of domain sizes is not uniform; the film shows a stripe structure at certain points (Figure 3, panels C and D). Within 20 min of the end of the second kinetic phase (Figure 3F), the film becomes solid and the focus progressively deteriorates (Figure 3, panels G and H). For IFABP-HL, the appearance of small domains started at a later time (Figure 3, panels J−L), but again close to the onset of the second kinetic process. Comparison of images at similar surface pressures (Figure 3, panels A and M) revealed similar domain sizes. At higher surface pressures (Figure 3, panels N−P), the injection of the helix-less variant induced a consistently more fluid film than the native protein, as judged by its motion in the BAM instrumentation.

IRRAS of DMPA. Acyl chain conformation is conveniently monitored in IR spectroscopy through the frequency of the symmetric CH_2 stretching mode [$\nu_s(CH_2)$]. It is well documented that values of <2850 cm^{-1} for this parameter indicate chains with high conformational order and that values >2853 cm^{-1} indicate the presence of a substantial level of gauche bonds (*19*). This parameter thus tracks acyl chain conformation through the entire compression curve for DMPA monolayers as shown in Figure 4A. The frequency appears initially at 2854 cm^{-1} at low Π values (gas, LE phases), changes cooperatively from 2853.5 → 2849.6 cm^{-1} during the LE-LC compression, and remains approximately constant at ~2849.2 cm^{-1} in the more ordered phases (LC, solid). The change in DMPA chain conformational order upon IFABP and IFABP-HL adsorption as monitored by $\nu_s(CH_2)$ is shown in Figure 4B. Prior to the injection, the lipid monolayer existed within the LE/LC coexistence regime and was characterized by $\nu_s(CH_2)$ of ~2852 cm^{-1}. Upon injection of wild-type IFABP, an initial rapid decline of the CH_2 stretching frequency to 2849.8 cm^{-1} was observed. The frequency stabilized at its final value of ~2849.2 cm^{-1} within 25 min, revealing DMPA acyl chains with a conformational order comparable to that in the LC or solid phases. In contrast, a much more gradual change of $\nu_s(CH_2)$ vs time was observed following IFABP-HL injection. At ~60 min, $\nu_s(CH_2)$ reached ~2850.5 cm^{-1} and never dropped below 2850 cm^{-1}. It is noted that the frequency precision for this

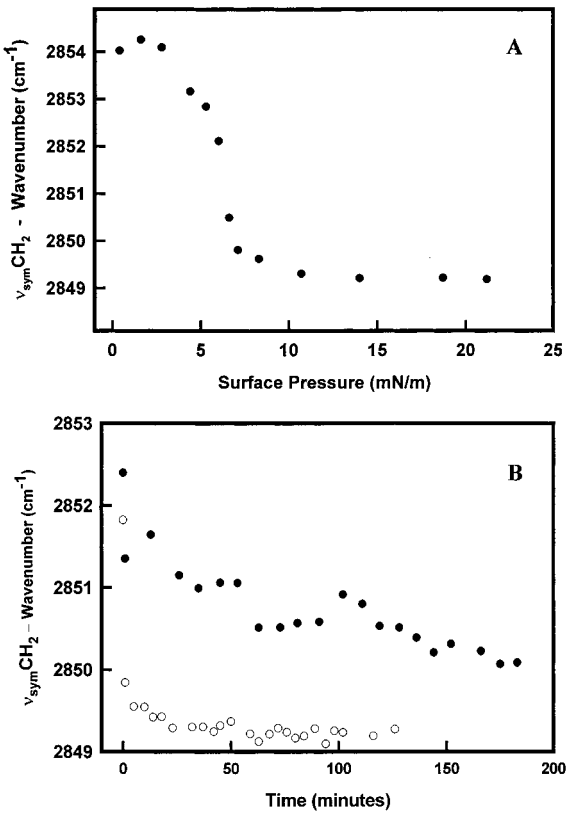

FIGURE 4: (A) DMPA monolayer isothermal compression monitored by IRRAS. The film was compressed intermittently. The ordinate scale is for $\nu_s(CH_2)$, the symmetric methylene stretching mode. (B) DMPA acyl chain conformational order change after IFABP or IFABP-HL injection, monitored by IRRAS at the A/W interface. The wild-type protein injection induced a rapid decrease in $\nu_s(CH_2)$ and resulted in a more ordered lipid conformation than the IFABP-HL. Legend: (●) IFABP-HL; (○) IFABP.

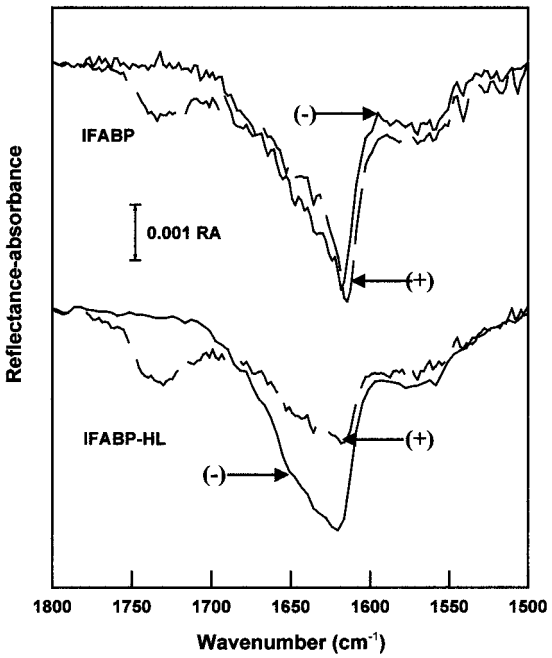

FIGURE 5: IFABP and IFABP-HL secondary structures in the presence (+, dashed line) and absence (−, solid line) of a DMPA monolayer at the A/W interface. The amide peak for the pure protein films is at ∼1617 cm^{-1}. In addition, the IFABP-HL spectrum shows more intensity at ∼1653 cm^{-1}. In the presence of lipids, the amide I peak of IFABP shifts down by ∼2 cm^{-1}. The 1735 cm^{-1} peak arises from the lipid carbonyl C═O stretching mode. The arrow represents 0.001 reflectance-absorbance(RA) units. The residual sharp peaks (usually < 0.0003 RA units) arise from uncompensated water vapor.

mode is better than ∼ 0.2 cm^{-1}. The observed final ∼1 cm^{-1} difference in $\nu_s(CH_2)$ for DMPA between the monolayers containing IFABP and IFABP-HL is thus substantial, and implies a much greater protein-induced conformational ordering of the lipid acyl chains by the wild-type protein.

IRRAS Determination of Protein Secondary Structure in Monolayers. Protein secondary structure at the A/W interface was determined from IRRAS measurements on a D_2O subphase. Overlays of the IRRAS spectra of IFABP and IFABP-HL in the presence and absence of DMPA monolayers are presented in Figure 5. The band at ∼1735 cm^{-1} arises from lipid C═O stretching. The presence of a DMPA monolayer shifts the peak position of the amide I band from 1619 to 1616 cm^{-1}. A pronounced shoulder at ∼1653 cm^{-1} is present in the IFABP-HL amide I envelope both in the presence and absence of DMPA.

The secondary structures adopted by wild-type IFABP and the helixless variant at the A/W interface in lipid monolayers differ from those in solution at room temperature, and also from each other. This is clear from examination of solution IR spectra from 25 to 70 °C, for both IFABP and IFABP-HL as shown in Figure 6. Both proteins possess predominantly antiparallel β-sheet secondary structures at room temperature as revealed by a low-frequency major band at ∼1630 cm^{-1} and a higher frequency minor component at ∼1685 cm^{-1} in agreement with the reported tertiary structures obtained by X-ray crystallography and NMR (*9*, *23*). IFABP-HL possesses additional intensity at ∼1655 cm^{-1}, for which it is difficult to make a secondary structure assignment. Two possibilities are random coil (although the frequency is several wavenumbers higher than normal) or a β-turn which for cyclic peptides gives rise to amide I bands sensitive to H-bonding and assigned throughout the whole frequency range for that mode (e.g., ref *24*). The assignment to secondary structures other than α-helical is made because there is no helix in the variant. The random coil is preferred based on the observation that the substitution of 17 residues in wild-type IFABP with a two residue (SG) linker, surprisingly introduces some flexibility into the molecule (*25*). Thus, the putative unordered structure observed in the IR measurements is likely to be related to the region close to that linker.

As shown in Figure 6, the thermal denaturation pathways are somewhat different for the two proteins. The random coil intensity for the IFABP-HL (Figure 6B) begins to increase at 60 °C and is followed by the appearance at 70 °C of a band near 1615−1620 cm^{-1} assigned to extended forms. For IFABP (Figure 6A) there is a much smaller initial increase in the random coil intensity; increased temperature results in the formation of the band arising from extended forms. In both cases, the denaturation is irreversible, as is evident from spectra marked 25c, which were acquired from denatured samples cooled back to that temperature. The spectra so obtained were distinctly different from the initial spectra in each instance.

Differences in lipid/protein interaction between the two lipid−protein films are also suggested by the observation of lateral heterogeneity in the film containing wild-type IFABP.

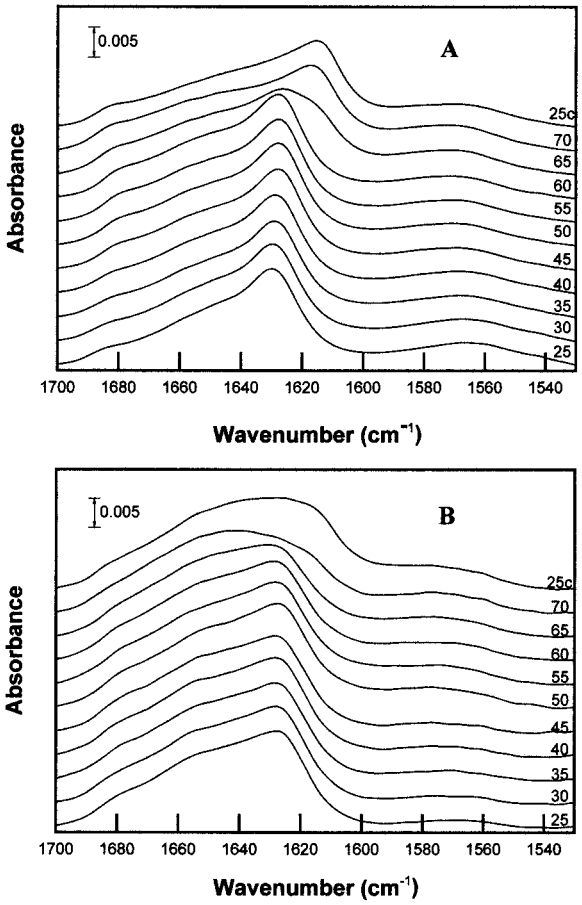

FIGURE 6: Bulk phase thermal denaturation of IFABP (A) and IFABP-HL (B) monitored by transmission IR. Spectra were collected every 5 °C and have been offset for clarity. The spectra marked 25c were taken from samples that were re-cooled to that temperature following thermal denaturation. The absorbance scale is indicated on each figure.

IRRAS spectra acquired at different sampling spots in the same experiment are displayed in Figure 7. In the top trace, a strong amide I band is accompanied by a weak CH_2 asymmetric stretching band intensity near 2919 cm^{-1}. In the lower trace, much stronger CH_2 stretching bands, both symmetric and asymmetric, are accompanied by a weaker amide I band. The integrated area ratio of the amide I envelope to the methylene modes is evidently much smaller compared to the same ratio in the upper trace. This implies that there exists a lateral distribution of the wild-type IFABP in the lipid film which produces protein-rich (top trace) and protein-poor (bottom trace) regions in the DMPA monolayer. Furthermore, since the IRRAS measurements reported here sample a large spatial area (the beam is ~1.5 cm in diameter at the surface), the inhomogeneities are apparently of macroscopic size, although the spatial distribution function remains to be evaluated.

It would be of interest to correlate the presence of protein-rich and protein-poor regions as measured by IRRAS and the banding pattern seen by BAM. However, with current instrumentation, the IRRAS and BAM measurements must currently be carried out on different Langmuir troughs, with different distance scales and data collection times required for measurements. Heterogeneous distributions were not detected for the helixless variant, suggesting but of course not proving, their absence in the film.

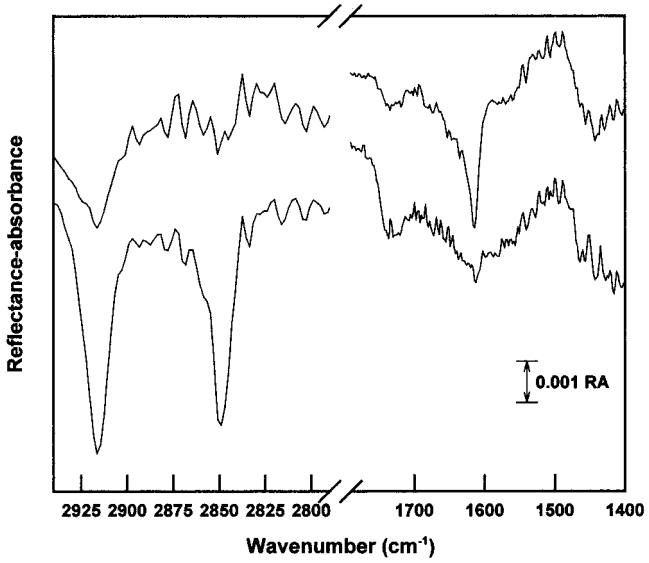

FIGURE 7: Heterogeneous distribution of IFABP in a DMPA monolayer detected by IRRAS. In the top trace, a strong amide I band from the protein is observed along with a weak lipid CH_2 stretching peak (protein-rich region). In the bottom trace, the relative intensities of these two modes are reversed (protein-poor region). The arrow represents 0.001 reflectance-absorbance (RA) units.

DISCUSSION

Previous studies of the kinetics of fatty acid transfer from IFABP to phospholipid membranes suggested that transfer occurred during protein−membrane interactions. Evidence for a collision-based mechanism included the proportional increase in the transfer rate of *n*-(9-anthroyloxy)-labeled free fatty acids from IFABP with increasing concentrations of acceptor membrane phospholipid, and the dramatic increases in transfer rate to membranes containing 25 mol % of anionic phospholipid. (*4*, *9*). In contrast, AOFA transfer from IFABP-HL to vesicles was not increased by either membrane concentration or acceptor vesicle charge (*13*), suggesting that protein−membrane interactions were either not occurring or that they were insufficient to modulate the rate of fatty acid transfer. It was also found that incubation of anionic vesicles with native IFABP, but not IFABP-HL was able to prevent the subsequent binding of cytochrome *c* to the membrane (*13*). All these observations are consistent with the membrane collisional mechanism proposed for FABP-assisted fatty acid transfer, and, in particular implicate the helix-turn-helix domain as a critical factor in the formation of the putative protein−membrane complex (*4*, *20*, *21*). The effects of structural changes in the lipid and protein components at various distance scales upon lipid/protein interaction are probed in the current experiments to assess directly these proposed IFABP/membrane interactions.

The current combination of approaches is advantageous as it eliminates problems involved with film transfer to solid supports. With our experimental design, water-soluble membrane proteins are injected into the aqueous subphase and allowed to interact with monolayers by diffusion. The surface activity of the protein, the formation of domains and the structural changes in both the lipid and protein constituents can be inferred from a combination of surface pressure measurements, BAM, and IRRAS.

The Π-time data for IFABP and IFABP-HL exhibited two kinetic phases that defined the surface pressure changes

(Figure 2). For IFABP, a 2−3 times faster rate of surface pressure change relative to IFABP-HL was observed for both stages. A reasonable interpretation of these data is that the initial (slow Π change) phase corresponds to protein binding to the membrane surface and/or direct interfacial adsorption and involves processes such as lipid conformational ordering, while the second phase (more rapid Π change) corresponds to processes such as protein conformational change and domain formation at the interface. The substantial contribution of membrane surface charge to the second phase is clear from the observation that this event is absent for the binding of the wild-type protein to zwitterionic DPPC.

The BAM experiments begin to define the interfacial structures formed when IFABP or IFABP-HL interact with anionic lipids. On the basis of studies of IFABP injection in film-free subphases and on the characteristics of pure DMPA domains (*22*), the condensed domains in Figure 3, panels A, B, L, M, and N are suggested to be lipid or at least lipid-rich domains. Two possible causes may lead to domain formation following protein adsorption onto lipid monolayers: specific lipid−protein interactions or nonspecific adsorption which reduces area accessible to the lipids. Condensed domains appeared in the IFABP-HL experiments at ∼70−80 min compared with 30 min following injection of wild-type protein. These time scales for domain formation are consistent with the slower onset of the second kinetic phase observed in the Π-time adsorption isotherms in Figure 2. Comparison of domain size distributions, average sizes and shapes at similar surface pressures reveals no obvious difference between IFABP and IFABP-HL. However, some differences in banding patterns are suggested by comparison of Figure 3, panels C and D with M and N. In addition, at later stages, injection of IFABP yielded a more solidly textured film (Figure 3, panels E−G) and a more rapid deterioration of focus compared with IFABP-HL (Figure 3, panels N−P). The films formed at long times following IFABP injection were rigid. This may be caused by three-dimensional microcrystallization of IFABP−DMPA complexes. In the IFABP-HL case, the film was less rigid and still exhibited substantial motion even at the end of the 3 h measurement period. IRRAS provides a molecular view of the effect of protein on lipid conformation. Prior to the protein injections, the DMPA monolayer was at the onset of LE/LC transition (see Figure 4A), as manifest by $\nu_s(CH_2)$ of ∼2852 cm^{-1}. This state of the monolayer is relatively poorly ordered and packed, since typically the CH_2 stretching frequencies increases from ∼2849 to ∼2854 cm^{-1} in the bulk phase during the gel−liquid crystal phase transition. Injection of wild-type IFABP has a strong, rapid ordering effect on the monolayer, lowering $\nu_s(CH_2)$ to ∼2849.8 cm^{-1} within a couple of minutes, followed by a slower further decrease of 0.6 cm^{-1} within ∼25 min (Figure 4B). The IR data thus suggest a very rapid initial lipid conformational ordering process. This event is difficult to explore thoroughly since it takes 5−8 min to acquire IRRAS data of adequate S/N ratio, and the pressure changes following IFABP injection occur more rapidly than this. The initial observation of condensed domains in the BAM experiment occurs at a time that roughly parallels the end of the initial decrease in $\nu_s(CH_2)$. We note that we are unable to detect domains smaller than about 10 μm in diameter with our current BAM apparatus. At times of >25 min, $\nu_s(CH_2)$ remained constant.

IFABP-HL showed a smaller change in $\nu_s(CH_2)$ from ∼2852 to 2850.5 cm^{-1} occurring over a longer (50−60 min) time period. At longer times, IFABP-HL never induced lipid conformational ordering as strong as in the wild-type protein within the observation period, consistent with the observation of a less rigid film in the BAM experiment, and in accord with the Π-time kinetic data.

A possible origin of the weaker effects induced by IFABP-HL comes from consideration of the protein charge. Like most other members of the FABP family, IFABP exhibits approximately equal overall positive and negative charges. However, LiCata et al. (26) have demonstrated surface charge polarity for the protein, with the top (helical domain) of the molecule more positive, and the "bottom" (barrel) of the molecule having a strong negative potential. Deletion of the helical domain in IFABP-HL results in the net loss of three positive charges, thereby reducing the interaction of this region of the protein with anionic monolayers.

In monolayer phases (Figure 5), the major amide I peak is observed at ∼1617 cm^{-1} , close to the position for thermally denatured protein (Figure 7) in the bulk phase for both proteins, and is assigned to extended or aggregated structures at the interface. Due to reduced signal-to noise ratios and the presence of residual water vapor in the IRRAS experiments with protein monolayers, detailed analysis of the Amide I band shape are not feasible. However, the IRRAS spectrum still provides qualitative information about protein secondary structure at the A/W interface unavailable by other methods. As in the bulk phase, the IFABP-HL amide I band possesses more intensity at ∼1653 cm^{-1} (perhaps arising from unordered structure) in the presence and absence of the lipid monolayer (Figure 5). However, since the extinction coefficients for different protein secondary structures are not necessarily the same (either in solution or in monolayers), the component of the amide I at 1653 cm^{-1} does not necessarily represent a large fraction of unordered forms in IFABP-HL.

A collisional mechanism involving membrane binding was proposed (*5*, *6*, *21*, *27*) for fatty acid transfer from IFABP to membranes. Previously, we used bulk phase FTIR to show that adipocyte FABP interacts with anionic membranes (*28*). Interactions of adipocyte FABP and IFABP with membranes have also been suggested by the results of a biochemical assay using competition between the FABP's and cytochrome *c* for membrane binding (*13*, *29*). In the present studies, we demonstrate directly the membrane-interactive properties of IFABP and IFABP-HL. The combination of surface pressure measurements, BAM, and IRRAS reveals a two step process, of which at least the second is electrostatic in nature. For wild-type protein, the interaction is characterized by an initial conformational ordering of the lipid acyl chains, the formation of distinct domains and the appearance of a rigid BAM film at long times. Deletion of the helical motif slows the time course of the initial stages of the interaction, suggested to be protein binding, accompanied by acyl chain ordering as well as the later stages of the process likely reflecting further conformational changes in the lipids and formation of lipid rich domains. The results directly demonstrate specific IFABP interactions with anionic membranes and support the hypothesis that the helix-turn-helix region of the protein is important for formation of the "collisional com-

plex", which promotes fatty acid transfer from IFABP to membranes.

ACKNOWLEDGMENT

We thank Gregory DeKoster and Ruth Steele for assistance with the preparation of Figure 1.

REFERENCES

1. Glatz, J. F. C., and van der Vusse, G. J. (1996) *Prog. Lipid Res. 35*, 243−282.
2. Thumser, A. E. A., and Storch J. (2000) *J. Lipid Res. 4*, 647−656.
3. Bass, N. M. (1985) *Chem. Phys. Lipids 38*, 95−114.
4. Hsu, K. T., and Storch, J. (1996) *J. Biol. Chem. 271*, 13317−13323.
5. Herr, F. M., Matarese, V., Bernlohr, D. A., and Storch, J. (1995) *Biochemistry 34*, 11840−11845.
6. Herr, F. M., Aronson, J., and Storch, J. (1996) *Biochemistry 35*, 1296−1303.
7. Hodsdon, M. E., and Cistola, D. P. (1997) *Biochemistry 36*, 1450−1460.
8. Hodsdon, M. E., and Cistola, D. P. (1997) *Biochemistry 36*, 2278−2290.
9. Hodsdon, M. E., Ponder, J. W., and Cistola, D. P. (1996) *J. Mol. Biol. 264*, 585−602.
10. Kim, K., Cistola, D. P., and Frieden, C. (1996) *Biochemistry 35*, 7553−7558.
11. Steele, R. A., Emmert, D. A., Kao, J., Hodsdon, M. E., Frieden, C., and Cistola, D. P. (1998) *Protein Sci. 7*, 1332−1339.
12. Cistola, D. P., Kim, K., Rogl, H., and Frieden C. (1996) *Biochemistry 35*, 7559−7565.
13. Corsico, B., Cistola, D. P., Frieden, C., and Storch, J. (1998) *Proc. Natl. Acad. Sci. U.S.A. 95*, 12174−12178.
14. McConnell, H. (1991) *Annu. Rev. Phys. Chem. 42*, 171−195.
15. Honig, D., and Möbius, D. (1991) *J. Phys. Chem. 95*, 4590−4592.
16. Möhwald, H. (1990) *Annu. Rev. Phys. Chem. 41*, 441−476.
17. Flach, C. R., Brauner, J. W., Taylor, J., Baldwin, R. C., and Mendelsohn R. (1994) *Biophys. J. 67*, 402−410.
18. Sakai, H., and Umemura, J. (1997) *Langmuir 13*, 502−505.
19. Mendelsohn, R., Brauner, J. W., and Gericke, A. (1995) *Annu. Rev. Phys. Chem. 46*, 305−334.
20. Wootan, M. G., and Storch J. (1994) *J. Biol. Chem. 269*, 10517−10523.
21. Kim, H. K., and Storch. J. (1992) *J. Biol. Chem. 267*, 77−82.
22. Wu, F. (1999) Ph.D. dissertation, Rutgers University.
23. Sacchettini, J., Gordon, J. I., and Banaszak, L. J. (1989) *J. Mol. Biol. 208*, 327−339.
24. Hollosi, M., Majer, Z. S., Ronai, A. Z., Magyar, A., Medzihradszky, K., Holly, S., and Fasman, G. D. (1993) *Biopolymers 34*, 201−207.
25. Steele, R. A., Emmert, D. A., Kao, M. E., Hodsdon, M. E., Frieden, C., and Cistola, D. P. (1998) *Protein Sci. 7*, 1332−1339.
26. LiCata, V. J., and Bernlohr, D. A. (1998) *Proteins 33*, 577−589.
27. Kim, H. K., and Storch, J. M. (1992) *J. Biol. Chem. 267*, 20051−20056.
28. Gericke, A., Smith, E. R., Moore, D. J., Mendelsohn, R., and Storch. J. (1997) *Biochemistry 36*, 8311−8317.
29. Smith E. R., and Storch, J. (1999) *J. Biol. Chem. 274*, 35325−35330.

BI002252I